Flow Turbulence Combust
https://doi.org/10.1007/s10494-018-9955-x

Mixing Characteristics of Non-Newtonian Impinging Jets at Elevated Pressures

Vincent Notaro[1] · Prashant Khare[1] · Jong Guen Lee[1]

Received: 26 January 2018 / Accepted: 19 June 2018

Abstract The effect of chamber pressure on the mixing characteristics of like-doublet impinging liquid jets is experimentally and numerically investigated for non-gelled and gelled hypergolic propellant simulants. The experiment uses planar laser induced fluorescence technique to investigate the mixing efficiencies of impinging liquid streams. It is found that mixing is enhanced for both gelled and non-gelled fluids as the pressure increases. However, gelled simulants generally result in poorer mixing as compared to their non-gelled counterparts, suggesting that pre-impingement conditions are important factors that determine mixing efficiency. To verify this hypothesis, high-fidelity direct numerical simulations, based on a state-of-the-art volume-of-fluid (VOF) method are conducted at elevated pressures for the gelled simulant, treated as a Herschel-Bulkley non-Newtonian fluid. It is found that the Sauter mean diameter (SMD) changes significantly, and approaches the SMD of non-gelled impinging jets if the incoming jets are either perturbed by a sinusoidal disturbance or a fully developed turbulent flow profile is introduced, explaining the experimental observations and confirming the hypothesis.

Keywords Non-Newtonian fluids · Impinging jets · Mixing efficiency · Volume of fluid

1 Introduction

Impingement of liquid jets is one of the most efficient methods for atomization and mixing, and have been widely used in a wide variety of applications, especially in propulsion and combustion systems. When two liquid jets impinge on each other, the dynamic head of the injected propellant destabilizes the liquid streams, creating a liquid sheet which disintegrates into ligaments and droplets under the action of aerodynamic, viscous, inertial,

✉ Prashant Khare
Prashant.Khare@uc.edu

[1] Department of Aerospace Engineering and Engineering Mechanics, University of Cincinnati, Cincinnati, OH 45221-0070, USA

Published online: 29 June 2018

and tensile forces [1]. Additionally, manufacturing simplicity and adaptable configurations enable impinging jets to achieve a wide range of fuel-oxidizer ratios and flow rates, making them an effective choice for propellant delivery. A commonly used configuration, known as like-doublet, is when two equal-sized orifices inject jets that impinge on each other, a schematic diagram of which is shown in Fig. 1. Doublet type injectors can be used with a variety of propellants including liquids, which can be Newtonian or non-Newtonian, gases, and gels [2–7].

Gelled propellants have been of particular interest for propulsion applications because they combine the variable thrust capabilities of liquid propellants with the handling and storage advantages of solid propellants. The benefits of gelled propellants are especially relevant to highly toxic hypergolic propellants. In such propellants, gelling alleviates the issues related to vapor toxicity and auto ignition, making them safer to store and handle. Hypergolic propellants can be effectively atomized and mixed using doublet injectors. However, there is a lack of sufficient understanding of the processes underlying the behaviors of impinging gelled propellants, especially with respect to their mixing characteristics at elevated chamber pressures. Therefore, this paper focuses on the impinging jet dynamics and mixing characteristics of gelled propellants in like-doublet injectors at elevated pressures.

Rupe [8] investigated liquid-liquid, non-reacting, doublet impinging jet mixing efficiencies for a range of parameters, including momentum ratio, impingement angle, pre-impingement distance, orifice area scale, and orifice area ratio. The mixing efficiency was empirically defined based on a weighted scaled deviation of the local mixture ratio to the nominal mixture ratio. Rupe [9] continued his work and refuted his previous hypothesis that optimum mixing occurs when the orifice area ratio and momentum rate ratio are both unity. Instead, it was concluded that a pair of impinging streams has its "most uniform configuration" that is, greatest mixing efficiency, when the ratios of the velocity heads and

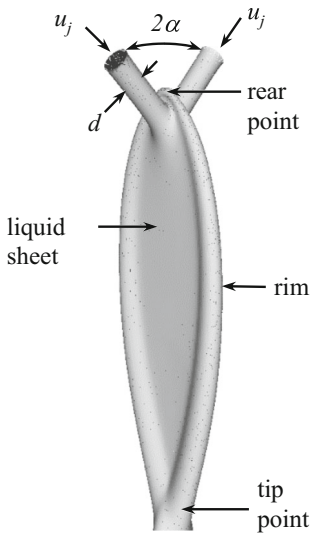

Fig. 1 Schematic diagram of doublet impinging jets

stream diameters is one. This ratio, known as the Rupe factor, can be applied over a range of impingement angles and area scales to optimize a pair of injectors.

Ashgriz et al. [10] conducted mixing studies with similar diameter orifices for miscible and immiscible, and dyed and non-dyed fluids. They concluded that at lower jet velocities with steady and smooth surfaces, the jets bounce off of one another and the fluids stay on their respective injected side. However, at higher jet velocities droplets cross each other at the impingement point. The bouncing and crossing phenomena are called reflective and transmitive atomization, respectively.

In addition to the abovementioned studies that addressed the effect of nozzle geometry on mixing in terms of orifice diameters, area scale and area ratios, Riebling [11] investigated the influence of nozzle geometry on mixing using orifice length-to-diameter ratio as the test variable. Using unlike impingement of equal diameter orifices, and constant impingement angle, pre-impingement distance and mixture ratio, it was concluded that mixing is unaffected by changes in orifice length-to-diameter values between 7 and 100. It was also found that mixing is unaffected for Reynolds number greater than 14,600.

All mixing investigations discussed in the previous paragraphs used patternators, a gridded collection device used to geometrically map spray distribution. Recently, techniques based on planar laser induced fluorescence (PLIF) have been applied to study impinging jet systems. Jung et al. [12] assessed the effectiveness of using PLIF technique for like-doublet injectors by comparing PLIF to patternators and phase doppler particle analyzer (PDPA) measurements to address signal linearity and laser extinction. They showed that laser extinction issues can be avoided if spray mass ranges are kept narrow and concluded that PLIF accurately mimics patternator measurements, but that is not the case with PDPA.

Yuan and Huang [13] used PLIF to correlate jet penetration percentage and mixing efficiency of like on like impinging jets. They used droplet dynamics to categorize mixing in two classes: (1) film-mixing control for open-rim sprays, and; (2) droplet-penetration control in fully-developed sprays. This was followed by another study by Yuan et al. [14] at increased ambient pressures of up to 1.0 MPa (145 psi). By comparing orifice sizes, penetration percentage, mixing efficiency and momentum flux, it was found that the mixing behaviors are related to the instability of the jets before impingement.

Currently, there exists a number of investigations that focus on mixing analysis of impinging liquid jets at 1 atm pressure. However, limited studies describe the mixing characteristics of like-doublet injectors at elevated ambient pressures for both non-gelled and gelled fluid injection. Therefore, the objective of this study is to quantify mixing between two fluid streams using PLIF at elevated chamber pressures for like-doublet injectors, for non-reacting, water and gelled hypergolic simulants. Additionally, high-fidelity direct numerical simulations are also conducted to provide detailed structures, droplet size distributions and sauter mean diameters corresponding to gelled impinging jets at pressures of practical significance.

2 Experimental & Numerical Setup

2.1 Experimental procedure and diagnostics

Two stainless steel injectors of orifice length-to-diameter ratio of 5, and orifice diameter of 0.508 mm (0.020 in) are used. The orifices are machined using EDM to minimize surface

roughness, and the diameters are verified to be within ±2% of the nominal dimensions using a microscope. Constant half impingement angle and pre-impingement distance are set at 30° and 5 mm (0.197 in), respectively. For all cases, impingement is aligned and checked before testing. Nozzle cavitation is monitored visually and avoided if possible.

Figure 2 shows the schematic of the experimental set-up to test like-doublet, impinging jets for gelled fluid. The injector assembly hangs in a high-pressure chamber rated to 5.17 MPa (750 psi). Nitrogen is used to pressurize the chamber and the injectors are fed with high pressure tubing. Flow is dispensed from 0.965 L (0.034 ft^3) hydraulic cylinders that are driven by pressurized 5.5 L (1.45 gal) carbon steel tanks with hydraulic oil. The hydraulic oil flow, that determines the flow rate of the gelled fluid is controlled with needle valves. Linear position transducers (UniMeasure LX-PA-25) are attached to the hydraulic cylinders and a LabVIEW program converts the dispensed volume to flow rate. For Newtonian fluids, instead of the hydraulic cylinders, flow is induced by back pressure from similar 5.5 L (1.45 gal) stainless steel tanks (not shown here), controlled with metering valves, and is measured with variable area flow meters (Brooks Instrument MT3809).

Tubing elements, such as check valves and filters are significantly far from the orifice exit to allow the flow to be fully developed. Rhodamine 6G is used to dye the gel simulant in two different concentrations, 3 mg/L (0.0568 ct/gal) and 6 mg/L (0.114 ct/gal). In order to quantify mixing, the same flow conditions are imaged with the aforementioned dye concentrations. The first image is obtained when both nozzles inject the dye with the weaker concentration, and in the second image, only one of the nozzles inject the dye with the stronger concentration. Mixing is then quantified based on the difference between the two images.

The working fluid for the Newtonian case is distilled water, with a density of 1000 kg/m^3(1.94 $slugs/ft^3$), viscosity of 1.002×10^{-3} Pa·s (2.09×10^{-5}(lbf ·s)/ft^2) and surface tension of 0.072 N/m (0.00493 lbf /ft). The base fluid for simulant gel is a 75% ethanol, 25% water mixture mixed with 0.1% carbomer (Lubrizol Carbopol 981A), which is known to exhibit low yield stress and negligible thixotropy. The base fluid is mixed

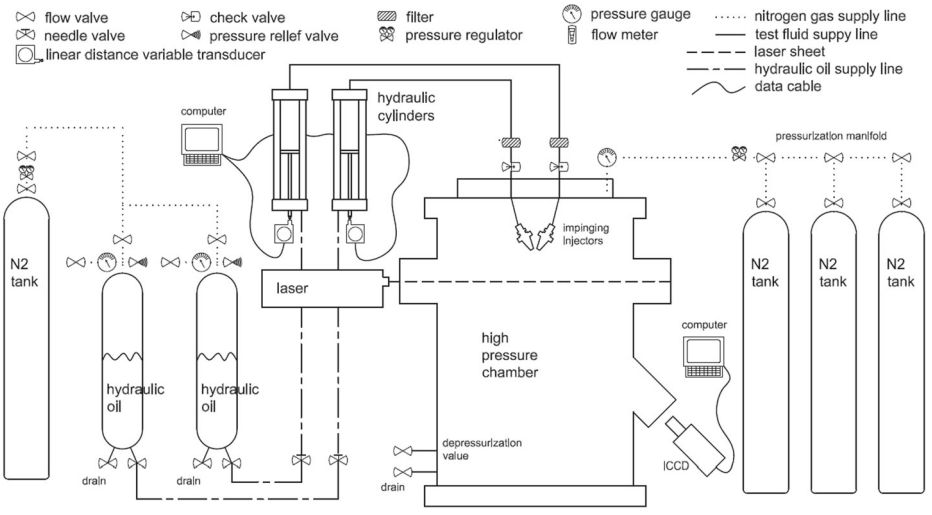

Fig. 2 Experimental setup for to investigate like-doublet impinging jets for Newtonian and non-Newtonian gelled simulants

with fumed silica (Cabot Corp. CAB-O-SIL TS-720) which acts as a thickening filler. The physical properties of the gelled fluid are a density of 866.9 kg/m^3 (1.68 slugs/ft^3) and a surface tension of 0.0255 N/m (0.00175 lbf/ft). A cup and cone arrangement of the rheometer (TA Instruments AR200) is used to determine the change of viscosity with applied shear. Fresh batches of gel are prepared and rheologically tested to maintain conformity with standard gelled hypergolic propellants (GHP) in terms of the relation of viscosity to shear rate. The rheometer offers torque control (0.0003 μN·m to 200 mN·m) with a resolution of 0.1 nN·m. The relationship between the dynamic viscosity versus shear rate is shown in Fig. 3. More details on material characterization are found in Fakhri et al. [15] and Ramasubramanian [16].

Shadowgraph, a technique that is used to characterize near- and far-field atomization processes is used to measure the breakup length. As shown in Fig. 4, breakup length is defined as the distance from the impingement point to the point where the sheet breaks off into ligaments. The light source for shadowgraphy technique used in this research is a Xenon nanopulser 737B, which is capable of emitting 5 mJ with a pulse duration of 10 ns. The light is collimated using a lens (ThorLabs LA1131 N-BK7, 1 in.-diam and 50 mm focal length), which is directed onto the optical access window of the high-pressure chamber and is focused onto a digital single-lens reflex camera (Nikon D7000 equipped with a 180 mm macroscopic lens). Typical settings for the camera are an exposure time of 1/6th of a second, an International Organization of Standardization (ISO) sensitivity setting of 1600, and an f stop of 4.5. Once the images are captured, they are processed using ImageJ software. For each flow condition, typically 100 images are obtained. Further details on this technique can be found in our previous paper [16].

To fluoresce the dye, a 10 Hz Nd:YAG laser with second harmonic generator emitting 532 nm light at 6.5 mJ per pulse (Continuum Surelite) is used. Optics trains generate a collimated laser sheet 45 mm by 2 mm with a 7 ns duration. Fluorescing spray images are captured at 50.8 mm (2.0 in) downstream of the impingement point by an ICCD camera (Princeton Instruments PI-MAX3) with 180 mm macro lens and 590 nm longwave-pass

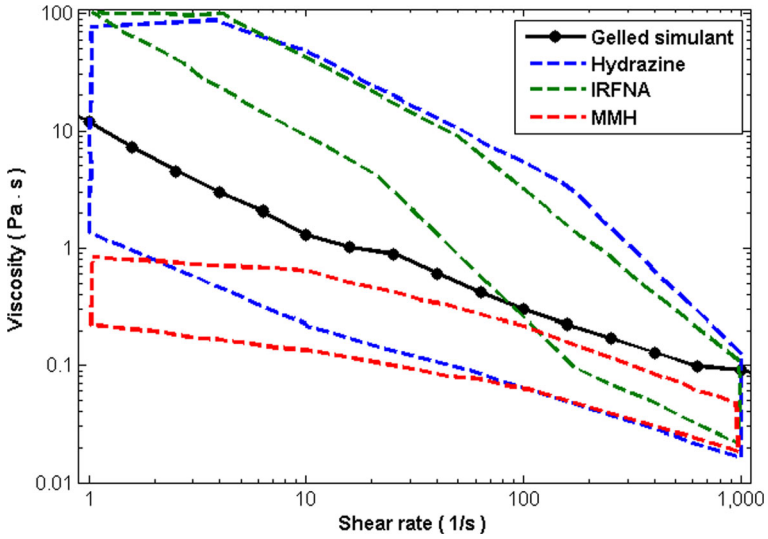

Fig. 3 Gelled simulant viscosity versus shear rate and ranges of existing gelled hypergolic propellants

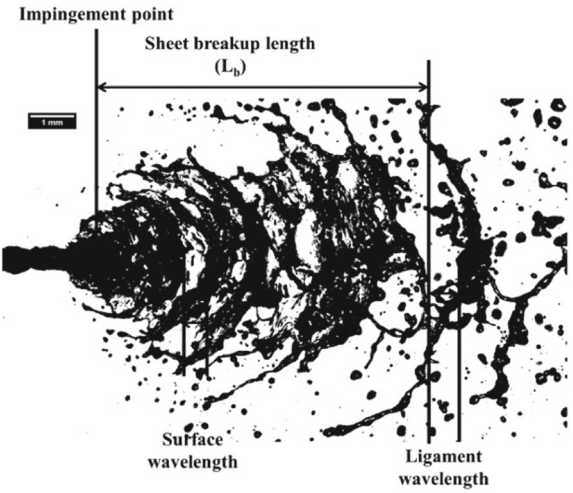

Fig. 4 A typical instantaneous image of a liquid sheet formed by two impinging jets issuing water jet (flow direction is from left to right) [16]

and 620 nm bandpass filters. The downstream imaging location is chosen such that only droplets are captured. The intensified charge-coupled device (ICCD) has a sensor of 1024 pixels by 1024 pixels in which each pixel covers roughly 0.05 mm (0.002 in). Images are taken at a 45° angle and perspective distortion is corrected using bicubic interpolation [17] projective mapping and a gridded plate (see Fig. 5). For each spray case, two sets of 200 images are acquired at steady-state conditions. Upon capturing, the background, which consists of noise from the ICCD and scattering of laser light from particles in the pressurized chamber, is subtracted from each collected image.

Fuel and total mass sprays are imaged and compared both qualitatively and quantitatively. This comparison is conducted by visually and numerically overlaying images. Based on the observations of Jung et al. [18], the overlay uses the center of mass of the spray as the reference point. Corresponding spray centers deviate by less than 30 pixels (1.5 mm) and 8 pixels (0.4 mm) in the horizontal and vertical directions, respectively. The alignment of the center of spray mass distribution corrects errors associated with the flow rate setting. Unbalanced flow rates introduce a small momentum imbalance that adds a sheet deviation angle. The local fluorescence signal is then related to the local mass of the spray, simplifying the data analysis because of the similarity of the working fluids. The fluorescence signal intensity is expressed as follows:

$$f_{x,y} = K I_{x,y} n_{x,y} = K I_{x,y} C V_{x,y} \tag{1}$$

where $f_{x,y}$ is the local fluorescence intensity, K the optical collection efficiency, $I_{x,y}$ the local laser intensity, $n_{x,y}$ the number of dye molecules, C the number concentration of dye, and $V_{x,y}$ is the local volume of the spray. Since the local laser intensity and collection

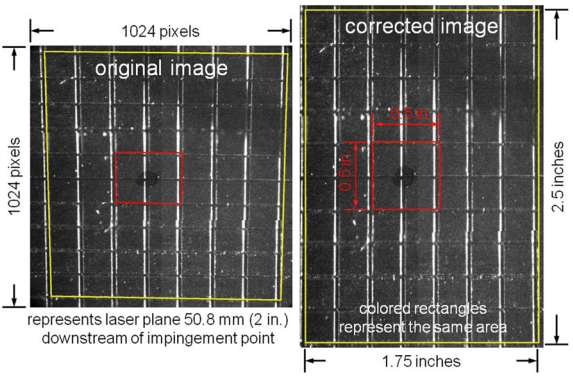

Fig. 5 Bicubic projective mapping correction on gridded plate and final image size

efficiency remains constant, the fluorescence intensity is directly related to the dye concentration and local volume of the spray. Dye concentration for each case is homogeneous. Normalizing the fluorescence signal by the dye concentration allows the comparison of fluorescence signals from the weaker and stronger dye cases. Since the two fluids are incompressible, the volume is related directly to the mass. Laser extinction is not present in our imaging technique. The fluorescence intensities of the densest spray region follow a Gaussian curve, as shown in Fig. 6. Extinction would be evident if the ends of the bell curve were uneven. The symmetry of the pixel intensities is maintained even though the laser runs through the plane of the liquid sheet.

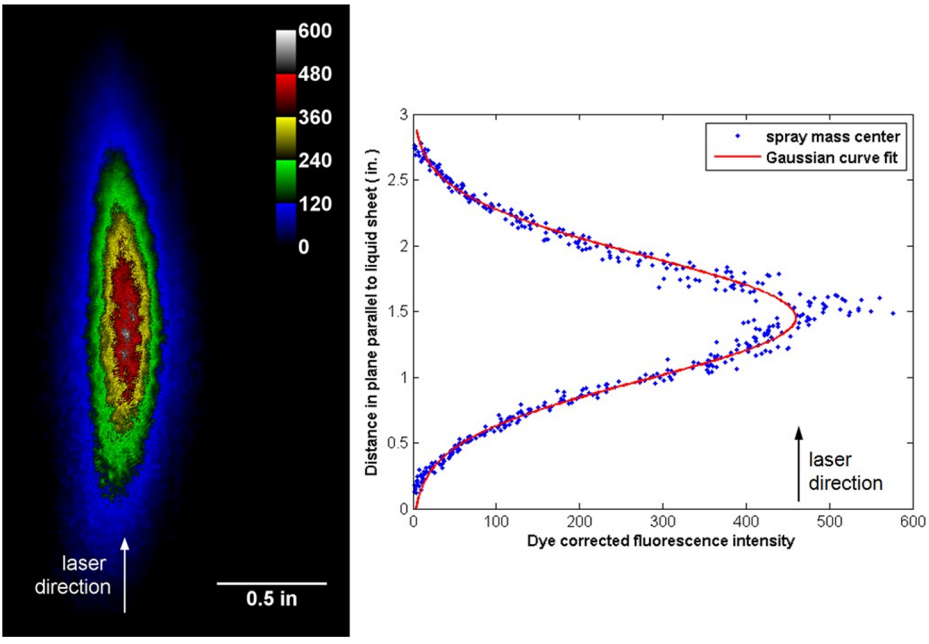

Fig. 6 Similar orifice diameter, equal momentum, like, water impingement at a jet velocity of 20.56 m/s and 0.69 MPa pressure conditions. The legend represents dye corrected florescence intensity

The mixing efficiency, E_m defined by Rupe [8, 9] and modified by others [10, 11, 13] is used here:

$$E_m = 100\left(1 - \left\{\sum_{0}^{N}\frac{\omega}{W}\frac{R - r_{x,y}}{R} + \sum_{0}^{\tilde{N}}\frac{\omega}{W}\frac{R - r_{x,y}}{R - 1}\right\}\right) \tag{2}$$

where ω and W are respectively the local and nominal mass flow rates of the spray, and $r_{x,y}$ and R are the local and nominal mixture ratios, respectively. The first summation represents the mass ratio and fuel mixture ratio scaled deviation of locations where fuel is needed. Correspondingly, the second summation is the mass ratio and oxidizer mixture ratio scaled deviation of locations where oxidizer is needed. Less deviations correspond to better mixing. Therefore, a mixing efficiency of one hundred means complete mixing and a mixing efficiency of zero means no mixing. The fluorescence intensity from two different averaged spray images are used. The image pixels are treated similar to cells in a patternator. The first image consists of the fluorescence of the spray when both jets are dyed at the weaker dye concentration. This represents the overall spray distribution. The individual and total pixel intensity represents local and total mass flow rates, respectively. The second image represents the fluorescence of the spray when just the fuel jet is dyed with the stronger dye concentration, and gives the fuel spray pattern and the fuel mass flow rate. Total mass spray images are used instead of oxidizer mass images to negate overlay issues of jet penetration movement of center of mass. The normalization and symmetry of the mixing efficiency definition allows either the oxidizer values to be in the numerator (Rupe) or the fuel values to be in the numerator (our study) for mixing ratios (see variables $r_{x,y}$ and R).

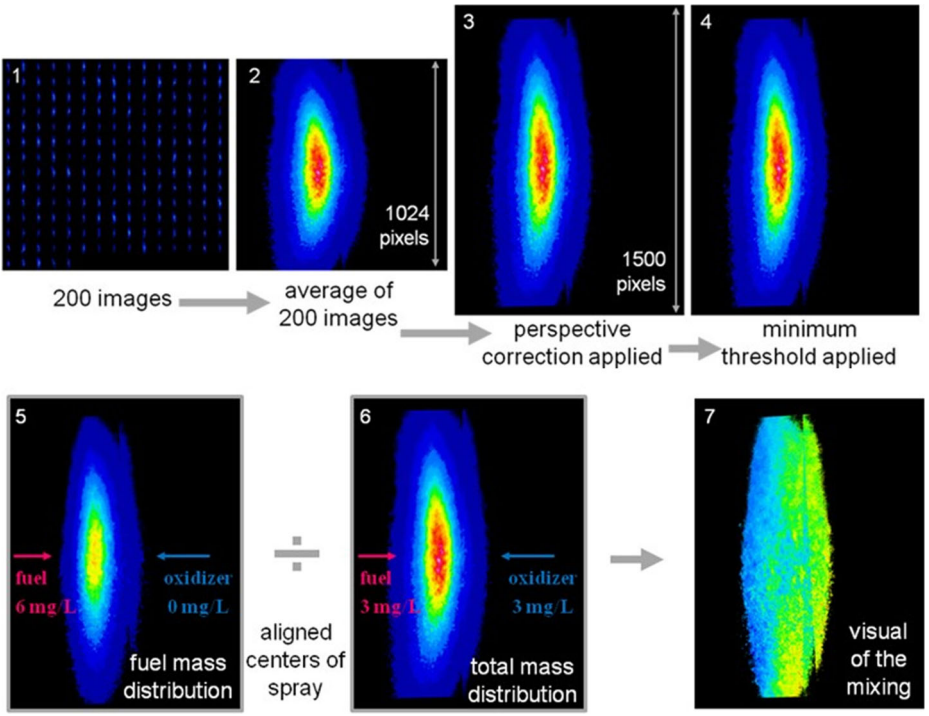

Fig. 7 Data reduction process for flow conditions in Fig. 6

Figure 7 shows an example of the data reduction process. Image "1" represents the spray when both the fuel and oxidizer working fluids are injected with the dilute dye solution (3 mg/L). The final image of this spray distribution is labeled "6". The image labeled "5" represents the spray distribution when one the fuel jet working fluid is dyed with the higher concertation (6 mg/L) and the oxidizer jet is undyed. It is created by repeating steps "2" through "4" on the corresponding images. The threshold applied to the averaged perspective corrected image eliminates false signals. Image "7" is generated by dividing "5" by "6". The division occurs pixel by pixel and gives the overlapping spray area. Image "7" presents a qualitative measure of the mixing process. The dye concentration is not corrected for and the direct division gives a mixture ratio distribution that is scaled by the dye concentration ratio. The vertical line to the right of the spray center masses in all of the pictures is the split line on the ICCD sensor.

2.2 Numerical framework

The numerical formulation of this multi-phase, multi-fluid problem, is based on three dimensional, incompressible, variable-density conservation equations with surface tension [19] and can be written as:

$$\frac{\partial \rho}{\partial t} + \nabla.(\vec{\rho u}) = 0 \tag{3}$$

$$\partial \left(\frac{\partial \vec{u}}{\partial t} + \vec{u}.\nabla \vec{u} \right) = -\nabla p + \nabla.(2\mu \overline{\overline{D}} + \sigma \kappa \delta_s n) \tag{4}$$

where $\vec{u} = (u, v, w)$ is the fluid velocity, $\rho = \rho(\vec{x}, t)$ the density, $\mu = \mu(\vec{x}, t)$ the dynamic viscosity, and $\overline{\overline{D}}$ is the deformation tensor defined as $D_{\text{ij}} = 1/2(\partial u_i/\partial x_j + \partial u_j/\partial x_i)$. The viscosity of the gel simulant is modeled as Herschel–Bulkley fluid. σ is the surface tension coefficient, κ and n are the radius of curvature and the unit vector normal to the interface, respectively. The Dirac delta distribution function, δ_s expresses the fact that the surface tension term is concentrated on the interface. This approach is called the "one-fluid" approach. To capture the multi-fluid interface, a volume-of-fluid (VOF) variable $c = c(\vec{x}, t)$ is introduced. It is defined as the volume fraction of the fluid in a given computational cell. The density and viscosity in each finite volume are linear functions of c, defined by

$$\rho(c) = c\rho_1 + (1 - c)\rho_2 \tag{5}$$

$$\mu(c) = c\mu_1 + (1 - c)\mu_2 \tag{6}$$

The theoretical formulation outlined above is solved numerically using a finite volume method augmented by an adaptive mesh refinement technique to improve the solution accuracy and efficiency. The adaptive octree spatial discretization allows for interface refinement. Further details on the numerical techniques can be found elsewhere [20]. This approach has been successfully applied and validated in our previous paper for a variety of configurations, including impinging liquid jets, and non-Newtonian liquid droplet breakup [21–26].

3 Results and Discussion

In the next few sections, we will discuss the effect of ambient pressure on mixing efficiency (defined by Eq. 2) for doublet injectors for water and gelled fluid. Detailed examination of the impinging jet behaviors for the gelled simulant will also be conducted using direct numerical simulations. Droplet size distributions, both number based PDF and Sauter mean diameters are calculated at elevated pressures to elucidate observations from experimental measurements. All cases have unity momentum ratios to give the best mixing results for like impingement of non-gelled and gelled fluids. A summary of all the test data is provided in Table 1.

3.1 Effect of ambient pressure on impinging water jets in a like-doublet configuration

As a first step we investigate the effect of ambient pressure on the mixing characteristics of impinging water jets. This study also serves as a validation and verification case for our

Table 1 Data of like impingement at 50.8 mm downstream of impingement point with injectors of L/D = 5 at $\alpha = 60°$ with 5 mm pre-impingement distance

Similar orifice diameters (0.508 mm) and MR = 1.0							
Working fluid – Water				Working fluid – Gel			
Chamber pressure (psi)	Jet flow rate (cm^3/min)	Jet velocity (m/s)	Mixing efficiency	Chamber pressure (psi)	Jet flow rate (cm^3/min)	Jet velocity (m/s)	Mixing efficiency
0	100	8.22	76.1	0	100	8.22	74.3
	150	12.33	81.7		125	10.28	73.1
	200	16.45	79.5		150	12.33	73.3
	100	8.22	77.0		175	14.39	73.8
	150	12.33	86.3		200	16.45	74.0
	200	16.45	88.4	250	100	8.22	86.0
	250	20.56	84.2		125	10.28	84.9
300	100	8.22	80.0		150	12.33	85.4
	150	12.33	81.6		175	14.39	80.6
	200	16.45	89.8		200	16.45	85.1
	250	20.56	86.1	380	100	8.22	82.6
500	100	8.22	83.9		125	10.28	83.5
	150	12.33	78.6		150	12.33	80.8
	200	16.45	89.3		175	14.39	83.9
		20.56	86.0		200	16.45	88.7
				500	100	8.22	84.6
					125	10.28	85.4
					150	12.33	87.9
					175	14.39	90.7
					200	16.45	87.6

experimental procedure. Figure 8 shows the mixing efficiencies as a function of chamber pressure. Also shown is data from Ashgriz et al. [10] with comparable injector configuration and operating conditions. Results indicate that mixing efficiencies measured in the current research effort are in excellent agreement with the published data, and follow similar trends for mixing at atmospheric conditions. Ashgriz et al. [10] did not acquire any data points at the jet velocities beyond 16.45 m/s at 0.1 MPa (1 atm) pressure because hydraulic flip causes jet alignment issues.

For a jet velocity of 8.22 m/s, as the ambient pressure increases, the mixing efficiency increases by 10.3% from 0.1 to 3.45 MPa. For most cases, any pressure increase above atmospheric results in better mixing. The monotonic increase in mixing at the lowest jet velocity (8.22 m/s) is attributed to a decrease in breakup length [16] and the longest contact time. Progressively shorter breakup lengths indicate an increase in turbulent dispersion that contributes to better mixing [10]. The contact time dictates the duration at which droplets can mix microscopically, thus longer contact times correspond to better mixing.

For velocities of 16.45 m/s and above, at chamber pressures greater than 0.69 MPa, the mixing efficiency stays constant. This is because the breakup length does not decrease as much at lower jet velocities [16], meaning the pre-atomization and post-atomization breakup regimes are roughly the same and contact time is fixed for a set velocity. The shorter contact time for the highest jet velocity explains why the extent of mixing is less than that of the jet velocity of 16.45 m/s. For the jet velocity of 12.33 m/s, mixing decreases after the initial jump from atmospheric pressure. This is due to the fact that this jet velocity is within the laminar to turbulent transition regime. The fluctuations of the jet are amplified by the increasing pressure [27]. This amplification reduces the contact area and time due to the inconsistent impact in this regime, thus reducing the extent of mixing.

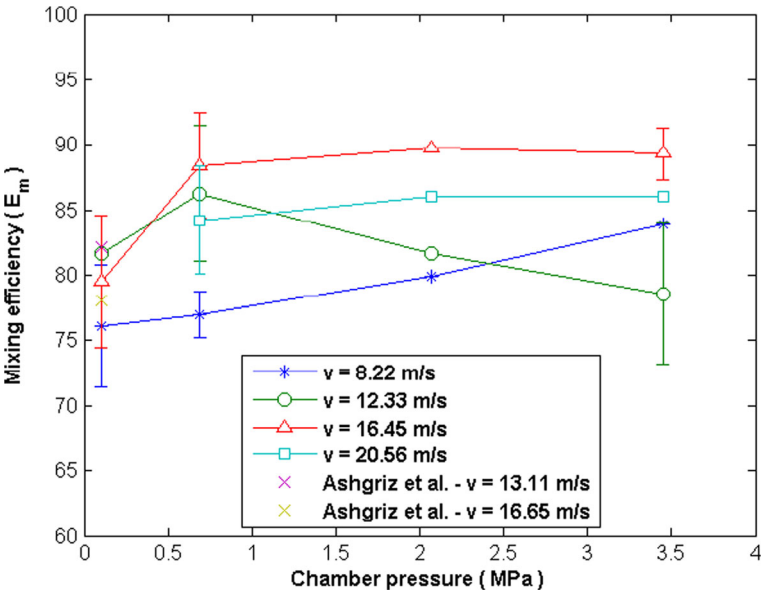

Fig. 8 Similar orifice diameter, equal momentum, like, water impingement and data from [10] ($d = 0.508$ mm, injector orifice $l/d = 5.4$). Velocity labels in the legend indicate single jet exit velocity. Error bars are 1 std. deviation

3.2 Ambient pressure effect on gelled fluids

Mixing efficiency data for gelled simulant are illustrated in Fig. 9. It is found that any pressure increase from atmospheric improves mixing. After the initial increase from 0.1 to 1.72 MPa, the mixing efficiency remains almost constant for jet velocities at or below 12.33 m/s and improves gradually for jet velocities above 14.39 m/s. For jet velocities higher than 14.39 m/s, the mixing efficiency monotonically increases with chamber pressure due to faster breakup. Higher jet velocities have higher kinetic energy, thus breakup takes place via impact wave mechanism [23], which further facilitates mixing. Regardless of the jet velocity, mixing efficiency remains constant for chamber pressures of 0.1 and 1.72 MPa. The efficiency range increases only at higher chamber pressures.

As the pressure increases, the drag experienced by the liquid sheet increases because of higher gas density. This leads to reduced liquid sheet sizes, and intensifies the breakup and atomization behaviors [28]. In addition to enhanced atomization and shorter breakup lengths at higher pressures, the shear-thinning nature of the gelled fluid leads to significantly enhanced turbulent dispersion, and thus higher mixing efficiencies. In summary, the increasing aerodynamic forces on the individual jets due to the increasing gas density contributes to enhanced mixing efficiencies at higher ambient pressures.

3.3 Droplet size distributions for gelled fluids and the effect of inlet velocity profile

To further investigate the effect of pre-impingement conditions on the impinging jet behaviors, high-fidelity direct numerical simulations are conducted. In addition to droplet size distributions, primary breakup lengths are calculated. The gelled simulant in the numerical

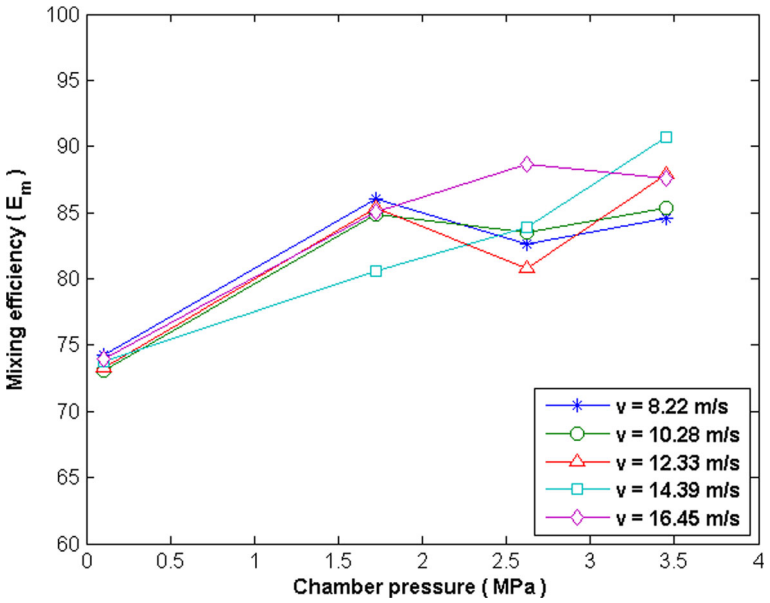

Fig. 9 Similar orifice diameter, equal momentum, like, gel impingement. Velocity labels in the legend indicate single jet exit velocity

calculations is treated as a Herschel-Bulkley type non-Newtonian fluid, whose properties are measured in the experiment and implemented in the current calculations, given by:

$$\mu = \frac{\tau_0}{\gamma} + K\gamma^{n-1} \tag{7}$$

where γ is the shear rate, the yield stress, $\tau_0 = 18$ Pa, the pre-exponent coefficient, $K = 6.99$, and power law index, $n = 0.345$. Calculations are conducted for $p = 0.1$-3.5 MPa. A thorough validation of non-Newtonian fluid behaviors with the current methodology can be referred to in our previous publications [21, 26, 29].

Figure 10 shows the time evolution of the liquid fraction when the non-Newtonian liquid jets impinge on each other at an operating pressure of 3.5 MPa, orifice diameters of 0.508 mm and an inlet velocity of 16.45 m/s with a parabolic profile at the inlet. Similar to Newtonian fluids, an impact wave is created at the impingement point, which travels downstream and destabilizes the liquid sheet. However, because the fluid is non-Newtonian, breakup of the liquid sheet is delayed and fragmentation takes place after significant stretching, which also explains the higher mixing efficiency for water as compared with gels (see next section). It should be noted that the gel simulant under consideration is shear thinning. Therefore, as the shear rate increases, its behavior becomes close to Newtonian fluids. Figure 11 shows the vorticity field corresponding to the liquid sheet evolution and subsequent fragmentation. It is observed that intense vorticity is generated at the impingement point and at all the locations where the liquid ligaments detach due to breakup.

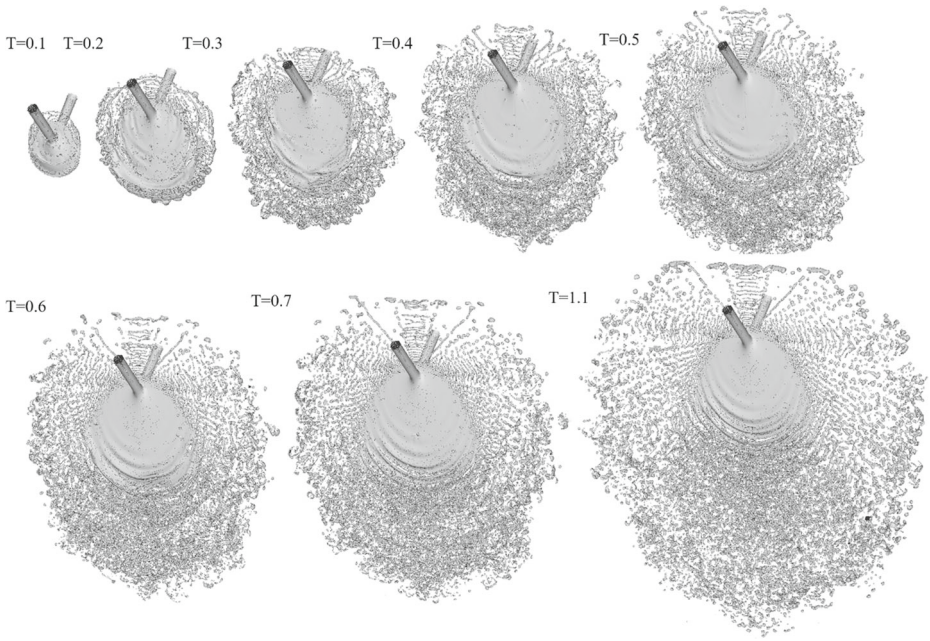

Fig. 10 Time evolution of the liquid fraction for impinging jets of the non-Newtonian gel simulant. $p = 3.5$ MPa, $d = 0.508$ mm, velocity = 16.54 m/s. Non-dimensional time, T = t/(d/velocity)

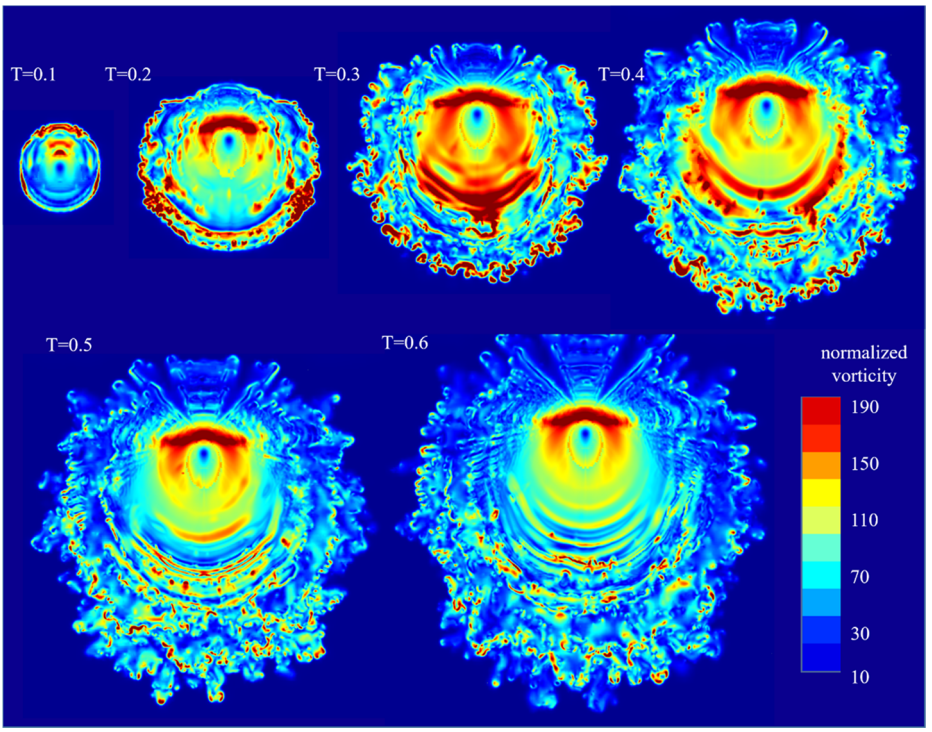

Fig. 11 Time evolution of vorticity field for impinging jets of the non-Newtonian gel simulant. $p = 3.5$ MPa, $d = 0.508$ mm, velocity $= 16.54$ m/s. Non-dimensional time, T = t/(d/velocity)

Figure 12 shows the droplet size distribution (skipping every eight symbols for clarity) corresponding to Fig. 10. The sauter mean diameter (SMD)[1] is 0.27 mm (neglecting the liquid sheet and the intact incoming jets). To assess the effect of inlet disturbances on the behaviors of two gelled jets impinging on each other, two more high-fidelity calculations are conducted by imposing sinusoidal disturbance at the inlet[2] and the other with a fully turbulent inlet profile given by the 1/7 law. The amplitude of sinusoidal perturbation was 1% of the inlet velocity and the frequency was 10 Hz. Table 2 presents a summary of SMD/D for both Newtonian and non-Newtonian fluids with different inlet velocity profiles. The SMD for the sinusoidal and turbulent inlet cases differ from the base case by 7.4% and 14.8% respectively, suggesting that at higher pressures pre-impingement processes are significant factors affecting the atomization behaviors and mixing characteristics. Further, for the same

[1] $\mathrm{SMD} = \int_{\infty}^{0} D^3 dN / \int_{\infty}^{0} D^2 dN$

[2] $U = U_0[1 + U' \sin(2\pi f t)]$, where U_0 is the base velocity, U' the amplitude of the disturbance, and f is the frequency of perturbation.

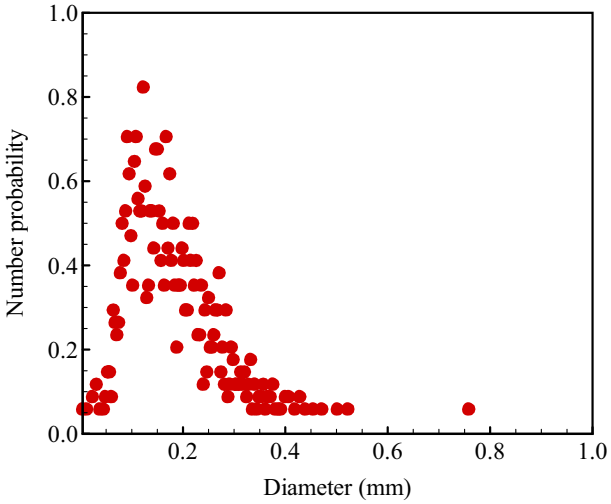

Fig. 12 Droplet size distribution corresponding to Fig. 10

conditions as Fig. 10, the SMD for the non-gelled (i.e., water) case is 0.19 mm as compared to 0.23 mm for the gelled case with a fully developed turbulent flow profile at the inlet. The number of droplets produced in the gelled case are, however, considerably more than the non-gelled case because of the shear thinning nature of the fluid. It is found that the primary breakup length of the liquid sheet is significantly smaller in the non-gelled case, larger fluid structures contribute to the enhanced SMD distribution.

The numerical studies confirm the mixing efficiency trends observed in the experiments. It is found that the breakup lengths reduce by up to 10% when pressure is increased from 0.1 to 3.5 MPa, which explains the increasing trend of mixing efficiency when the ambient pressure is increased—longer contact times at higher pressures correspond to better mixing.

3.4 Comparison of non-gelled and gel simulant

Figure 13 shows the comparison of three exit jet velocity cases for experiments conducted on gelled and non-gelled simulants. At the lowest jet velocity (8.22 m/s), the gelled simulant exhibits better mixing especially for the higher ambient pressures. In this case, the pre-impingement jet perturbations of the water jets are greater than that of the gelled fluid; increasing disturbances in the pre-impingement jets tends to decrease mixing extent [10].

Table 2 Sauter mean diameter for Newtonian and non-Newtonian fluids with different inlet velocity profiles

Fluid	Newtonian	Non-Newtonian		
Profile	Parabolic	Parabolic	Parabolic with sinusoidal disturbance	1/7 power law (represent fully developed turbulent flow profile)
SMD/D	0.37	0.53	0.49	0.45

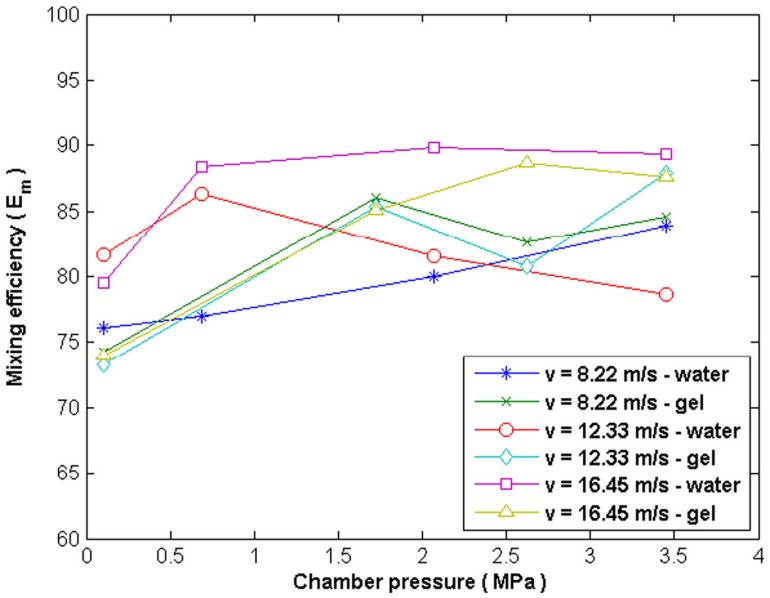

Fig. 13 Like-doublet, water versus gel mixing comparison

At a jet velocity of 12.33 m/s at lower ambient pressures, the non-gelled simulant has a better mixing efficiency, but at elevated pressures, the mixing efficiency becomes less than that of the gelled simulant. This is because at lower pressures, even though jet perturbations are larger for the non-gelled fluid, the momentum carried by the jets is greater due to water's higher density. This momentum increase causes breakup faster and increases turbulent dispersion, resulting in slight increase in the mixing efficiency. In addition, the gelled simulant produces more stable sheets, resulting in greater breakup lengths [15] that decreases turbulent dispersion in the post-atomization regime, which is known to significantly affect the extent of mixing [10]. For the highest injection velocity case (16.45 m/s), the mixing efficiency of the non-gelled mixture is always greater than that of the gelled mixture, irrespective of the chamber pressure. The momentum of water for comparable jet velocities is 15.5% greater than that of the gelled mixture, and hence the better mixing efficiency. The momentum difference is due to the density difference of the two fluids.

In summary, for a given jet velocity, the non-gelled fluid has a greater momentum due to its higher density and generally more jet turbulence than that of the gelled counterpart. At comparable lower jet velocities and even with lower momentum, the gelled mixture produces better mixing because of its more stable jet stream. However, as jet velocity increases, the mixing enhancement due to momentum exchange becomes dominant, and the mixing efficiency of water jets is higher as compared to the gelled fluid, even with more stable streams.

4 Conclusions

In this paper, mixing efficiencies of non-gelled and gelled impinging jets are experimentally numerically determined using PLIF and high-fidelity DNS calculations. The effectiveness

of mixing is enhanced as pressure increases because of reduction in primary breakup lengths, confirmed by the numerical simulations. Gelled simulant generally results in poorer mixing than the non-gelled simulant, suggesting the momentum carried, and more importantly, pre-impingement jet conditions are significant factors that determine the mixing efficiency. To confirm this experimental observation, simulations were conducted for three different inlet velocity profiles; parabolic, parabolic with sinusoidal disturbance, and a fully developed turbulent flow profile. Sauter mean diameters were calculated based on these high-fidelity calculations, which quantitatively confirmed the atomization behaviors observed in experiments - as the pressure increases, preimpingement conditions, such as inlet disturbances, and velocity profiles (which is a manifestation of the nozzle internal dynamics) play an important role in determining their dynamics and mixing efficiencies.

Acknowledgements The authors would like to gratefully acknowledge Dr. Ralph Anthenien, the contract monitor for supporting this research effort. The authors are also grateful to Dr. Stéphane Popinet for allowing them to use his VOF and AMR algorithms.

Funding Information This work was supported by the United States Army Research Office under the Multi-University Research Initiative (MURI), contract number W911NF-08-1-0124.

Compliance with Ethical Standards

Conflict of interest The authors declare that they have no conflict of interest.

References

1. Anderson, W.E., Ryan, H.M., Santoro, R.J.: Fundamental mechanisms of combustion instabilities: impinging jet injector atomization. In: Yang, V., Anderson, W.E. (eds.) Instability, Liquid Rocket Engine Combustion, pp. 215–246, AIAA Progress in Astronautics and Aeronautics (1995)
2. von Kampen, J., Alberio, F., Ciezki, H.K.: Spray and combustion characteristics of aluminized gelled fuels with an impinging jet injector. Aerosp. Sci. Technol. **11**, 77–83 (2007). https://doi.org/10.1016/j.ast.2006.08.006
3. Negri, M., Ciezki, H.: Atomization of Non-Newtonian fluids with an impinging jet injector: influence of viscoelasticity on hindering droplets formation. In: 46th AIAA/ASME/SAE/ASEE Joint Propulsion Conference & Exhibit. American Institute of Aeronautics and Astronautics (2010)
4. Ciezki, H., Robers, A., Schneider, G.: Investigation of the spray behavior of gelled jet-A1 fuels using an air blast and an impinging jet atomizer. In: 38th AIAA/ASME/SAE/ASEE Joint Propulsion Conference & Exhibit. American Institute of Aeronautics and Astronautics (2002)
5. Madlener, K., Ciezki, H., von Kampen, J., Heislbetz, B., Feinauer, A.: Characterization of various properties of gel fuels with regard to propulsion application. In: 44th AIAA/ASME/SAE/ASEE Joint Propulsion Conference & Exhibit. American Institute of Aeronautics and Astronautics (2008)
6. Heislbetz, B., Madlener, K., Ciezki, H.: Breakup characteristics of a newtonian liquid sheet formed by a doublet impinging jet injector. In: 43rd AIAA/ASME/SAE/ASEE Joint Propulsion Conference & Exhibit. American Institute of Aeronautics and Astronautics (2007)
7. Yang, L., Fu, Q., Zhang, W., Du, M., Tong, M.: Spray characteristics of gelled propellants in novel impinging jet injector. J. Propuls. Power **29**, 104–113 (2012). https://doi.org/10.2514/1.B34551
8. Rupe, J.: The liquid-phase mixing of a pair of impinging streams. Progress Report 20-195 (1953)
9. Rupe, J.: A correlation between the dynamic properties of a pair of impinging streams and the uniformity of the mixture-ratio distribution in the resulting spray. Progress Report 20-209 (1956)
10. Ashgriz, N., Brocklehurst, W., Talley, D.: Mixing mechanisms in a pair of impinging jets. J. Propuls. Power **17**, 736–749 (2001). https://doi.org/10.2514/2.5803

11. Riebling, R.W.: Effect of orifice length-to-diameter ratio on mixing in the spray from a pair of unlike impinging jets. J. Spacecr. Rockets **7**, 894–896 (1970). https://doi.org/10.2514/3.30067
12. Jung, K., Koh, H., Yoon, Y.: Assessment of planar liquid-laser-induced fluorescence measurements for spray mass distributions of like-doublet injectors. Meas. Sci. Technol. **14**, 1387 (2003)
13. Yuan, T., Huang, B.: Effects of momentum rate on the mixing of the spray of doublet impinging jets. In: ILASS Americas, 23nd Annual Conference on Liquid Atomization and Spray Systems. Ventura (2011)
14. Yuan, T., Chen, C., Chen, Y.-D., Huang, B.: The observation of the atomization and mixing of doublet-jets impinging sprays at elevated ambient pressures. In: ICLASS 2012, 12th Triennial International Conference on Liquid Atomization and Spray Systems. Heidelberg (2012)
15. Fakhri, S., Lee, J.G., Yetter, R.A.: Effect of nozzle geometry on the atomization and spray characteristics of gelled-propellant simulants formed by two impinging jets. At. Sprays **20**, 1033–1046 (2010). https://doi.org/10.1615/AtomizSpr.v20.i12.20
16. Ramasubramanian, C., Notaro, V., Lee, J.G.: Characterization of near-field spray of nongelled- and gelled-impinging doublets at high pressure. J. Propuls. Power **31**, 1642–1652 (2015). https://doi.org/10.2514/1.B35305
17. Burger, W., Burge, M.J.: Digital Image Processing an Algorithmic Introduction Using Java. Springer, Berlin (2008)
18. Jung, K., Yoon, Y., Hwang, S.-S.: Spray characteristics of impinging jet injectors using imaging techniques. In: 36th AIAA/ASME Joint Propulsion Conference and Exhibit. American Institute of Aeronautics and Astronautics (2000)
19. Pópinet, S.: An accurate adaptive solver for surface-tension-driven interfacial flows. J. Comput. Phys. **228**, 5838–5866 (2009)
20. Khare, P.: Breakup of Liquid Droplets (2014)
21. Ma, D., Chen, X., Khare, P., Yang, V.: Atomization and breakup characteristics of liquid sheets formed by two impinging jets (2011)
22. Chen, X., Khare, P., Ma, D., Yang, V.: Impinging jets and droplet dynamics. arXiv:1110.3356 (2011)
23. Chen, X., Ma, D., Yang, V., Popinet, S.: High-fidelity simulations of impinging jet atomization. At. Sprays **23**, 1079–1101 (2013). https://doi.org/10.1615/AtomizSpr.2013007619
24. Tomar, G., Fuster, D., Zaleski, S., Popinet, S.: Multiscale simulations of primary atomization using Gerris. Comput. Fluids **39**, 1864–1874 (2010)
25. Khare, P., Yang, V.: A study on the breakup of water droplets. Submitt. to Physics of Fluids (2018)
26. Khare, P., Yang, V.: Breakup of non-Newtonian liquid droplets. In: 44th AIAA Fluid Dynamic Conference (2014). https://doi.org/10.2514/6.2014-2919 10.2514/6.2014-2919
27. Lee, J.G., Ramasubramanian, C., Notaro, V.: Mixing analysis of like doublet injectors in high pressure environments for gelled propellant simulants. In: 50th AIAA/ASME/SAE/ASEE Joint Propulsion Conference (2014). https://doi.org/10.2514/6.2014-3584
28. Yasuda, N., Yamamura, K., Mori, Y.H.: Impingement of liquid jets at atmospheric and elevated pressures: an observational study using paired water jets or water and methylcyclohexane jets. Proc. R. Soc. A Math. Phys. Eng. Sci. **466**, 3501–3526 (2010)
29. Khare, P., Yang, V.: Newtonian and non-Newtonian liquid droplet breakup: child droplet statistics. In: Proceedings of the ICLASS 2015, 13th Triennial International Conference on Liquid Atomization and Spray Systems (2015)